Acoustically driven manipulation of microparticles and cells on a detachable surface micromachined silicon chip

Jingui Qian, Graduate Student Member, IEEE, Jifeng Ren, Wei Huang, Raymond H. W. Lam, and Joshua E.-Y. Lee, Senior Member, IEEE

***Abstract*—Particles and cells can be patterned and moved (i.e., manipulated) precisely using acoustically driven techniques. To date, application of acoustic particle manipulation has been limited to plain surfaces. There is much potential for applying acoustic manipulation techniques to surfaces with microfabricated structures for high-throughput sensing. But adding thin film structures could alter manipulation characteristics compared to a plain surface. Using a two-chip setup that allows the wave generating device to be reused, we study the feasibility of acoustofluidic micro-manipulation on a surface-micromachined silicon (SMS) chip. The SMS chip is a complex superstrate with generic thin-film structures fabricated by patterning and etching multiple layers of thin films, with properties meant to represent a broad range of microfabricated devices. We report notable alterations in the particle separation distances on the SMS chip compared to a bare silicon superstrate, which we attribute to a change in wave type through a comparison of different superstrates prepared. We demonstrate a high cell viability after acoustic manipulation of live cells on the SMS chip. The results herein demonstrate the possibility of integrating a suite of microfabricated sensors on a chip with acoustically driven manipulation capabilities for multiplexed sensing and analysis for bio-applications.**

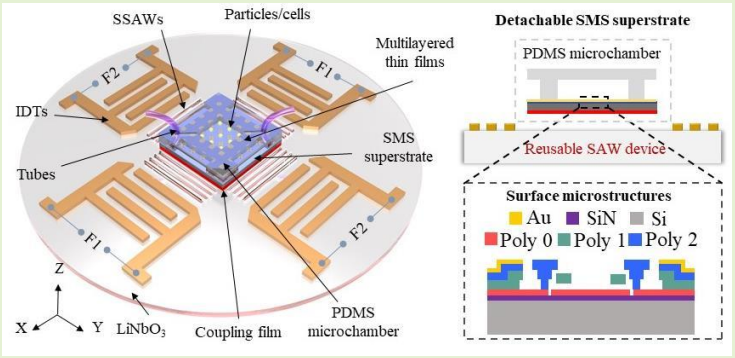

***Index Terms*—Cell patterning, cell manipulation, acoustic tweezers, surface acoustic wave, acoustofluidics, Rayleigh wave, polysilicon surface micromachining**

I. Introduction

PRECISION manipulation of microparticles and cells plays a critical role in fundamental biological analyses and medical applications. One example is the separation of circulating tumor cells from human blood cells, which has relevance for clinical analysis [1-3]. Acoustofluidic platforms for particle manipulation have received increasing attention recently. As a method, this approach is contactless, low in power consumption compared to optical tweezers [4], label-free, pollution-free, and has good biocompatibility [5-12].

Manuscript received October 13, 2020; accepted XX X, 2021. Date of publication XX X, 2020; date of current version XX X, 2020. The work was supported by grants from the Research Grants Council of Hong Kong under project number CityU 11218118. (Corresponding author: Joshua E.-Y. Lee)

Jingui Qian is with the Dept. of Electrical Engineering, City University of Hong Kong, Hong Kong (e-mail: jinguqian2-c@my.cityu.edu.hk).

Jifeng Ren, Wei Huang and Raymond H. W. Lam are with the Dept. of Biomedical Engineering, City University of Hong Kong, Hong Kong (e-mail: jf.ren@my.cityu.edu.hk; whuang42-c@my.cityu.edu.hk; rhwlam@cityu.edu.hk).

Joshua E.-Y. Lee is with the Dept. of Electrical Engineering and also the State Key Lab. of Terahertz and Millimeter Waves, City University of Hong Kong, Hong Kong, and also with the Institute of Microelectronics, Agency for Science Technology & Research, Singapore (e-mail: josh.lee@cityu.edu.hk).

In many biological applications, it is desirable for some parts of the analytical setup to be disposable while remaining cost-effective. In the case of acoustic tweezers, this has involved separating the microfluidic device from the piezoelectric acoustic transducer by fabricating the microfluidic device on a separate chip [13]. To prevent cross contamination, device components in direct contact with bio-samples are discarded after experiment [14]. By designing the two parts to be detachable when needed, the piezoelectric surface acoustic wave (SAW) device for generating the acoustic wave can be reused [15-17]. Most examples of such two-chip acoustically driven devices can be found in droplet-based fluidic handling functions such as concentrating and separating particles or cells [18-22]. In these setups, particles or cells are concentrated to a single point by traveling waves propagating on the superstrate as Lamb waves. A recent finding has showed that adding a thin metal layer on a silicon superstrate converts Lamb waves to Raleigh waves, which is preferred for droplet-based particle concentration [23].

Much less reports are two-chip acoustically driven devices that can pattern and move (i.e., manipulate) particles or cells in a matrix or an array. Two excellent examples are described in [24-25], which demonstrate detachable acoustofluidic devices for particle separation and fluorescence-activated cell sorting.

As in the case of single-device implementations [4], the particles or cells are kept in a microfluidic chamber for manipulation to be realizable. Instead of using traveling waves that interact with a droplet in particle concentration experiments, particle manipulation involves standing waves inside a sealed microfluidic chamber. To date, two-chip manipulation experiments have been limited to only simple bare superstrates [16, 26]. Applying such acoustic manipulation methods to microfabricated chips containing an array of devices could enable the integration of high-throughput cell handling and sensing functionalities. Such a microfabricated chip would comprise multiple layers of thin films, which may be patterned and etched by surface-micromachining techniques, yielding a superstrate that is much more complex than a simple bare superstrate. Given that adding just a thin metal layer is enough to alter the property of a traveling acoustic wave [23], a complex superstrate like a surface-micromachined silicon (SMS) superstrate would have notable effects on the standing acoustic wave and the performance of particle manipulation. To date, there are no reports on applying acoustic manipulation to an SMS superstrate and what difference may arise compared to bare superstrates. As such, this work seeks to characterize the performance of particle manipulation on an SMS superstrate and also demonstrate the feasibility of cell manipulation on such complex superstrates.

The aim of this work is to demonstrate the feasibility of acoustically driven manipulation of floating particles on a multilayered surface-micromachined device, which can have its own electrical and electronic functions. The SMS superstrate in this work has been processed with five layers of thin films that were patterned and etched, and that represent generic micro-structures that could be used for sensing. We have employed a thin polymer film of Polydimethylsiloxane (PDMS) as our choice of the coupling agent for the two-chip device among various liquid lubricants reported in the literature [26]. The PDMS coupling film allows detachability of the SMS chip from the SAW device and also provides reasonable acoustic coupling. We have successfully demonstrated two-dimensional (2D) manipulation of various types of particles on the SMS chip. To examine the effect of the surface micro-structures on acoustic manipulation, we compared the particle separation distances tested on different superstrates prepared. We have analyzed the moving velocity of the particles on the SMS superstrate in relation to particle size and density, frequency and input power level of the RF signals. Finally, we have successfully attempted to pattern and manipulate live tumor cells on the SMS superstrate.

II. Materials And Methods

A. Fabrication of integrated acoustofluidics device

To fabricate the SAW device, different interdigitated transducer (IDT) patterns were fabricated on a 128° Y-cut Lithium Niobate (LN) piezoelectric wafer (CETC Deqing Huaying Electronics Co., Ltd, China) using standard photolithography and lift-off techniques. This involved deposition of a metal stack (Cr/50 Å, Au/600 Å) by E-beam evaporation. Standard soft lithography (SU-8 2025, MicroChem) was used to fabricate the PDMS microchamber (height: 50 μm, width: 1200 μm) connected to two channels (width: 200 μm) on opposite sides. Next, both the PDMS microchamber and a PDMS coupling layer (thickness: 35 μm) were respectively plasma bonded to the topside and backside of the SMS chip (fabricated by MEMSCAP® using the PolyMUMPs™ process). A pair of vias were created through the PDMS around the ends of each microchannel using a 0.6 mm home-made punch to form an inlet and an outlet. Before each experiment, the superstrate (prepared with the PDMS chamber and coupling layer) was provisionally adhered to the SAW delay line by thermal bonding, as described in our previous research [26]. These steps allow a strong enough bond between the SMS superstrate and the LN substrate, but the bond is impermanent such that the SMS superstrate can be peeled off undamaged and does not leave any residue that is difficult to clean off. The detail fabrication process was explained in Fig. S1.

B. Particles and cells sample preparation

To demonstrate acoustic patterning and manipulation, polystyrene (PS) and silica particles (DAE Scientific, Tianjin, China) of various diameters (5 μm, 9 μm and 13μm) were diluted in deionized (DI) water (0.5 mg/mL for PS and 1 mg/mL for silica). Tween 20 (Sigma-Aldrich), as a non-ionic surfactant (detergent), was mixed into DI water (0.002%-0.003%) to avoid the adhesion of the particles on the PDMS wall. An early-stage residual clean (75% ethanol) was conducted before each experiment.

The human breast cancerous cell line MDA-MB-231 was obtained from ATCC (Manassas, VA). The cells were cultured in a high-glucose Dulbecco's modified Eagle's medium (DMEM; Invitrogen, Carlsbad, CA) supplemented with 10% fetal bovine serum, 0.5 μg/mL fungizone (Invitrogen), 5 μg/mL gentamicin (Invitrogen), 100 unit/mL penicillin, and 100 μg/mL streptomycin. The cells were maintained in an incubator at 37 °C, saturated humidity and 5% CO_2 in air. When the cells reached ~80% confluence, 0.25% trypsin-EDTA was used to re-suspend the cells with a cell concentration of 3×10^5 cells/mL. In the cell experiment, the fabricated PDMS microchamber was pre-coated with pluronics F-127 (Sigma-Aldrich) for 1 hour to avoid cell attachment on the channel walls.

C. Cell viability test

Cell viability tests were performed by flowing the cells through the acoustofluidic device at a rate of 100 μL/min with standing SAW (SSAW) applied (with an excitation of 35 dBm at 19.3 MHz). LIVE/DEAD Cell Imaging Kit (488/570) (R37601，Thermal Fisher) solution (1 mL), mixed with MDA-MB-231 cell culture medium (3 mL) to form an imaging solution, was added to the MDA-MB-231 cells after centrifugation. We divided the mixed solution into two parts. One part of the cell solution (2 mL) was injected and flowed through the microchamber with the SSAW applied for about 20 min, followed by imaging under a confocal microscopic for examining the percentage of living cells (ex/em 488/515 nm) and dead cells (ex/em 570/602 nm). The other half of the 2 ml cell solution was likewise imaged in the same way after incubating for about 20 min as the control group.

D. Measurement setup

The performance of the SAW device was tested using a

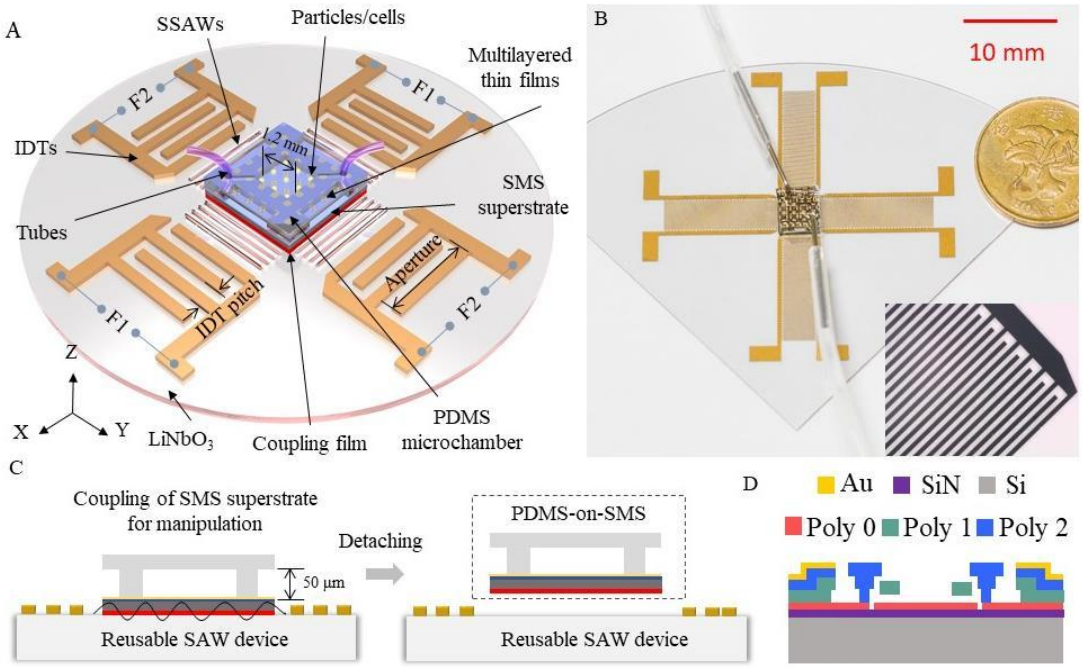

Fig. 1. (A) Perspective schematic of the integrated acoustofluidic device for manipulating microparticles and cells on a SMS superstrate; (B) Optical image of the proposed device with a Hong Kong fifty-cent coin as a size reference. Inset: captured parts of a 200 µm pitch IDTs imaged under a microscope; (C) Schematic to explain the proposed strategy to reuse the SAW device between experiments while changing the superstrate. Note: Only the standard IDTs are illustrated here. (D) Side view schematic showing the various thin film layers (five) on the SMS superstrate and illustration of a processed structure.

network analyzer (E5061A, Agilent, USA). Two signal generators (E8244A PSG-L series and E4438C ESG, Agilent) provided two pairs of input RF signals that were gained up via two power amplifiers (Mini Circuits ZHL-5W-1, 5-500 MHz) powered by a direct current supply (3 A, 24 V DC). Particles and cells were infused into the microchamber by a home-made syringe pump. An early-stage residual clean of the syringes was performed before each new round of experiments. The excess heat generated by RF inputs was dissipated using an aluminum heat sink. The whole device was placed on the stage of an upright microscope (AM73515MT8A, Dino-Lite, Taiwan) for monitoring and recording the results. The surface temperature was measured using a commercial industrial infrared thermometer (AT 380, XIMA, China), with a calibrated maximum deviation of ± 0.3°C. The fluorescence images of the tumor cells were captured under a confocal microscopic (Leica Confocal SP8 Microscope, Leica) for cell viability assays.

III. Working Mechanism

A. A two-chip plug-and-play acoustofluidic platform

Fig. 1(A) provides a schematic diagram of the two-chip acoustofluidic platform for manipulating particles and cells on a detachable SMS superstrate. SSAWs were generated though two pairs of IDTs perpendicular to each other. The SAW propagation direction of each pair of IDTs was offset by 45° relative to the x axis, such that the elastic and piezoelectric properties along both orthogonal axes of wave propagation were similar [10]. The half wavelength of the SSAW is equal to the IDT pitch (which corresponds to the IDT period as indicated in Fig. 1(A). We fabricated several SAW devices with different IDT pitches to vary the resonant frequency (corresponding wavelengths: 200 µm, 400 µm, and 600 µm). Each IDT comprised 40 pairs of electrodes. In addition, broadband chirped IDTs that comprised 26 pairs of electrodes were also designed for particle manipulation based on the frequency shifting method. The width and spacing of the electrodes of the chirped IDTs were designed to increase linearly from 50 µm to 75 µm with increments of 1 µm, corresponding to a SAW wavelength range from 200 to 300 µm. The aperture of the IDTs in all cases was kept at 4.4 mm to ensure that the microfluidic chamber area (1.2 mm by 1.2 mm) coincided fully within the acoustic field. The SMS superstrate was diced to an area of 5.4 mm by 5.4 mm, fitting nicely within the delay line (5.5 mm) between the IDTs. The SMS superstrate has been processed with five layers of thin films on the top surface of a silicon base. The deposited and etched thin films on the superstrate included an insulation layer of 0.6 µm thick silicon nitride, a 0.5 µm thick polysilicon layer for electrical routing (Poly 0), 2 µm thick polysilicon as the first structural layer (Poly 1) layer, 1.5 µm thick polysilicon second structural layer (Poly 2) layer, and 0.5 µm thick metal layer. The side view schematic in Fig. 1 (D) depicts a generic freestanding structure fabricated on the SMS superstrate. Fig. S2 shows the design pattern of a surface-micromachined device fabricated on the SMS superstrate. A PDMS microchamber (height: 50 µm, width: 1200 µm) with an inlet and an outlet was bonded on the topside surface of the SMS superstrate. We reduced the thickness of the sidewall (down to 1 mm) to decrease the acoustic attenuation through the PDMS chamber walls, but the bonding areas at the four corners were made wider (2 mm) to enhance the bonding strength between the PDMS chamber and superstrate surface.

We employed a thin polymer film (PDMS) as the coupling agent for such device, which provides simultaneous benefits of efficient acoustic wave transmission, long-term stability (i.e.,

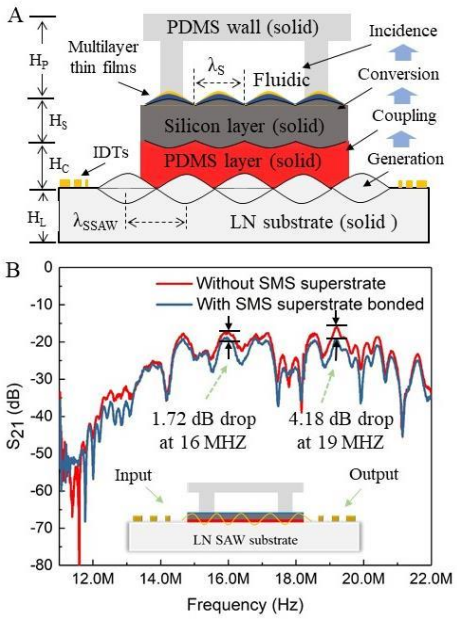

Fig. 2. (A) Sketch (not to scale) showing the material type of each part to explain the transmission of SSAW on the SAW substrate into the SMS superstrate. (B) Measured transmission efficiency S_{21} across the delay line via a pair of chirped IDTs with and without the SMS base bonding onto the SAW substrate.

chip does not move during the experiment), and allows the chip to be detached from the SAW after experiments [26]. As diagrammatized in Fig. 1(C), after applying thermal treatment to the whole device, the PDMS-on-SMS chip can be temporarily adhered to the SAW substrate by Van der Waals forces. After each experiment, the superstrate can be peeled off without damaging the SAW device that can be reused for the next experiment. An assembled plug-and play acoustofluidic device is captured in Fig. 1(B), with a Hong Kong fifty-cent coin as reference of its actual size. The inset is a zoom-in partial view of the SAW IDTs. To compare against the SMS superstrate, we also prepared and tested another two setups, which are described in S3 of the supplementary material. These include (1) a two-chip setup involving a simple bare silicon superstrate encased in a PDMS microchamber (Fig. S3 (a)), (2) a single-chip setup where the PDMS microchamber is directly bonded on the LN SAW device substrate (Fig. S3 (b)). These two additional setups were employed to compare the separation distance of pressure nodes on (1) a bare silicon superstrate, and (2) the LN substrate in a single-chip setup, as well as to compare the respective particle moving speeds on the different superstrates and setups tested.

B. Transmission and conversion of acoustic waves

As illustrated in Fig. 2(A), the SSAW was generated on the LN substrate and a fraction of the acoustic energy leaks into the SMS superstrate via the coupling layer. Typically, the Raleigh wave from the substrate is transformed into a Lamb wave in a bare silicon superstrate [27]. However, it has been reported that simply depositing a metal film layer transforms the Lamb wave back to a Raleigh wave according to Laser Doppler Vibrometer measurements [28]. Similar conversions may apply to standing waves as well, though this has yet been verified. In our patterning experiments, we have observed notable differences in the separation between pressure nodes on the SMS superstrate compared to a bare silicon superstrate. We attribute these differences to the type of waves involved: standing Raleigh wave (SSAW) vs. standing Lamb wave (SLW). We compared the average separation distance between particles patterned on a bare silicon superstrate versus silicon superstrates with one or two thin film layers, up to multiple layers of thin films (as in the case of the SMS superstrate). The LN substrate had a thickness (H_L) of 500 μm, the PDMS

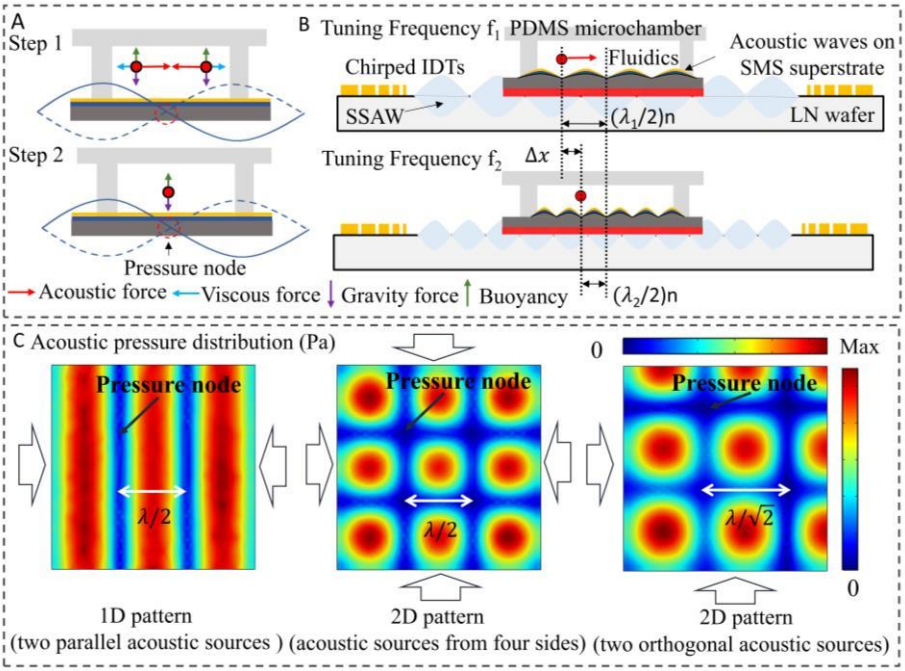

Fig. 3. (A) Four external forces emerged in the particles movement (1) and trapping step (2). (B) Principle of particles manipulation using a chirped IDT based on the strategy of frequency shifting. (C) Simulated pressure field distribution by generating acoustic waves from different sides. Generating waves from both sides along one axis yields 1D patterning lines (left). Generating waves from all four sides yields a 2D checkerboard pattern (middle). 2D checkerboard patterns can be also set up by generating waves from two-orthogonal sides (right).

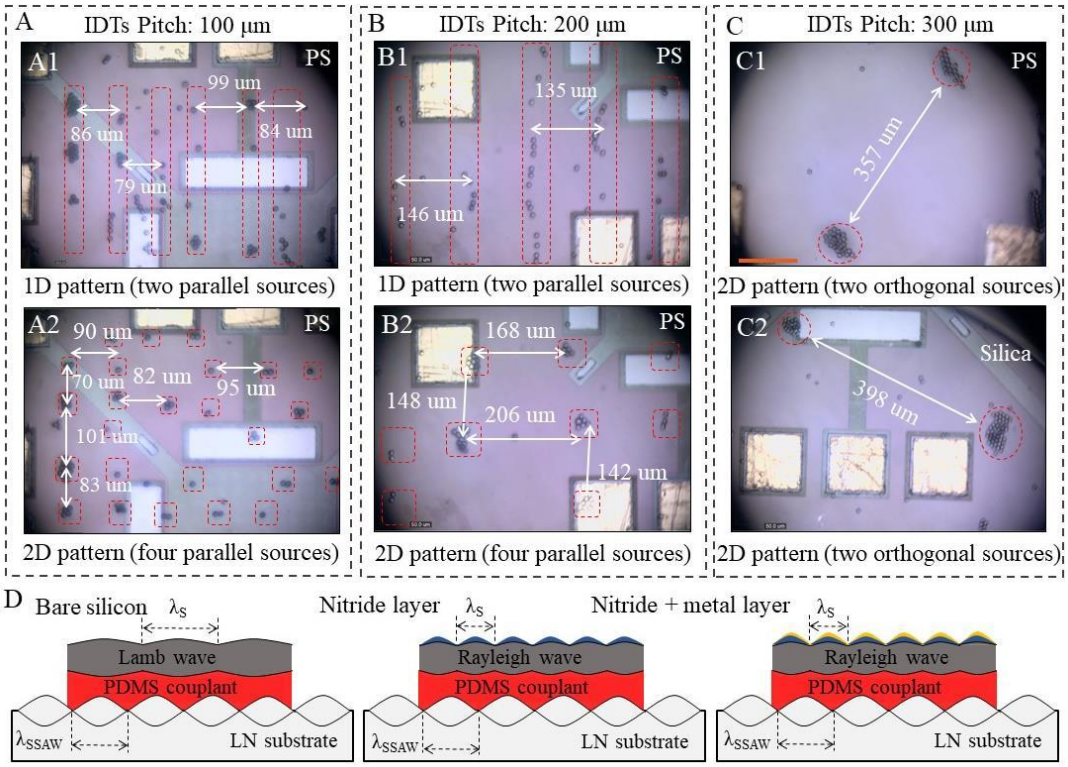

Fig. 4. Patterning of 9 μm PS and silica microbeads using standard IDTs. (A) Patterning of the PS particles with 100 μm pitch IDTs, the distance of between the parallel lines is about 70-100 μm; (B) Patterning of PS microbeads with 200 μm pitch IDTs, the distance between parallel lines is about 140 to 200 μm; (C) 2D patterning of the PS and silica microbeads with 300 μm pitch IDTs after one pairs of orthogonal SSAWs treatment, the distances of two nodes is about 350 to 400 μm. (D) Sketches shows the SSAW transmission from the substrate into the thin polymer film (couplant) and succeeding the various superstrates. Showing the excitation of (1) a Lamb wave for bare silicon, (2) a Rayleigh wave for nitride coating, (3) a Rayleigh wave for nitride and metal coating. Scale bar: 100 μm.

coupling layer had a thickness (H_C) of 35 μm, the silicon body of the SMS superstrate had a thickness (H_S) of 600 μm, and the PDMS microchamber structure had an outer height of about 2-3 mm.

To probe the acoustic coupling between the SAW device and SMS chip, we measured the transmission coefficient (S_{21}) to compare the insertion loss with and without the SMS superstrate bonded on the SAW delay line. As shown in Fig. 2 (B), the measured S_{21} verifies the generation of a broadband excitation frequency range from 13.3-19.95 MHz. The observable drops in transmission (at 16 MHz and 19 MHz) were observed in different SAW devices bonded to different superstrates. Such drops reveal leakage of a fraction of acoustic energy from the SAW device into the SMS base, which provides the means for setting up a stationary acoustic field within the superstrate to realize particle manipulation on the SMS superstrate.

C. Patterning and manipulation principle

When the acoustic field is generated on the chip, as shown in Fig. 3 (A), four types of external forces act on the particles to move and trap these particles [28]. The balance between gravity and buoyancy determine the equilibrium position of a particle along the vertical axis [29]. Along the horizontal axis, both the acoustic radiation force (ARF) and viscous force act on the particles, the formula and analysis of which are described in S4 of the supplementary material. It has been reported that particles with a diameter larger than 3 μm are pushed toward the nearest pressure nodes, as the ARF normally surpasses the viscous force [30] for particles at these scales.

By exciting different combinations of IDTs, one-dimensional (1D) and two-dimensional (2D) acoustic field patterns may be generated as illustrated in the acoustic field simulations depicted in Fig. 3 (C) using COMSOL. The image on the left of Fig. 3 (C) shows the resulting 1D pressure distribution by generating acoustic waves simultaneously on both sides of the manipulation space (where the microchamber is placed) along one axis. The pressure nodes are periodically spaced at half the acoustic wavelength (λ/2) in the form of a series of parallel nodal lines. Generating acoustic waves from all four sides of the manipulation space results in a 2D pressure distribution in the form of a checker box matrix as shown in the middle image of Fig. 3 (C) due to the superposition of standing waves along the x and y axes. The distance between adjacent nodes along either axis is also thus λ/2. It is also possible to set up a 2D pressure distribution by generating acoustic waves from two sides rather than four, as depicted in the right figure of Fig. 3(C). In this configuration, the distance between nodes along either axis is equivalent to λ/√2 [4]. Hence, the periodic spacing between particles aggregating at pressure nodes is determined by the frequency of the input signal.

There are two means of manipulating particles by acoustic forces: phase shifting and frequency tuning [31]. The latter was preferred for our two-chip platform involving a SMS superstrate owing to the multiple thin film layers giving rise to non-uniform wave attenuation and interchanging between different vibration modes between different parts of the chip. These factors make control using the phase difference between

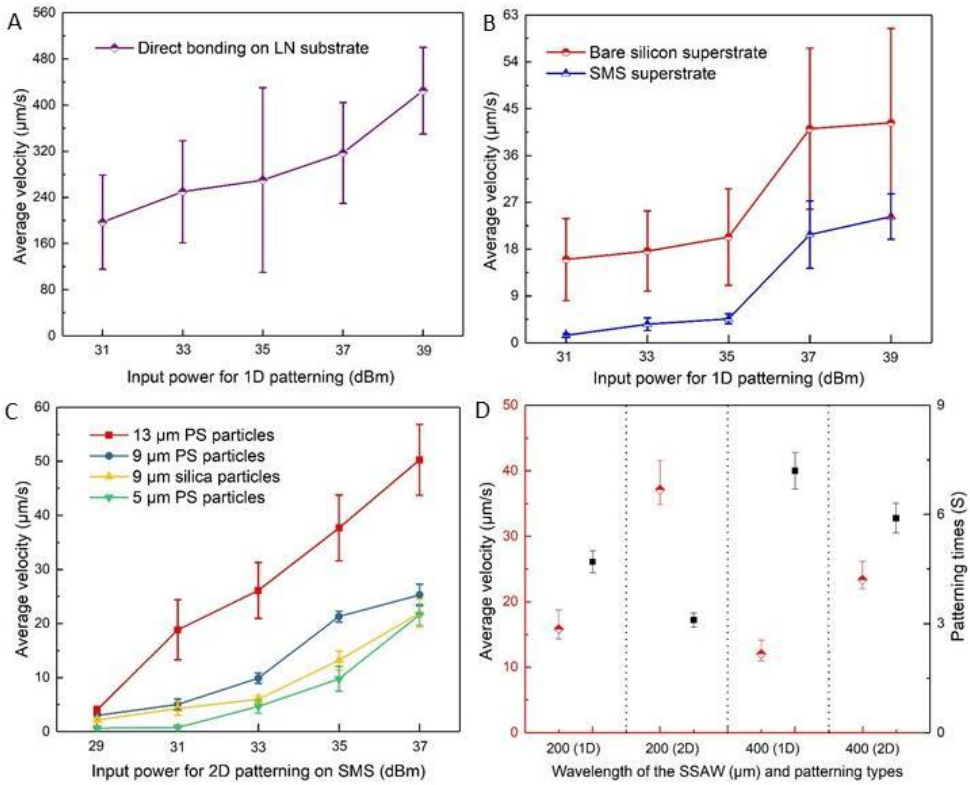

Fig. 5. (A-B) Measured average velocities of microbeads with increased input power from 31 dBm to 39 dBm during 1D patterning, where the particles were manipulated directly on the SAW device, on a bare silicon superstrate (400 μm thick), and SMS superstrate (600 μm thick). (C) Comparison of the average velocities for different particle diameters and densities with increased input power from 29 dBm to 37 dBm during 2D patterning; (D) Measured average velocities and required patterning/settling time to investigate in relation to the wavelength of the SSAW on the LN substrate to illustrate the effect of excitation frequency on the acoustic radiation force. N ≥ 3.

sources difficult. Frequency on the other hand is characteristic (dependent on the medium and type of wave) and is not disrupted by attenuation or wave conversion. Fig. 3(B) depicts the method of frequency tuning for particle manipulation. The amplitude of relative manipulation displacement is directly proportional to the order number of the acoustic pressure node [28], which can be derived using the same formulation applied to common bare superstrates [26].

IV. Results And Discussion

A. 2D patterning of various microbeads

We compared the 2D particles patterns on four different superstrates, to reveal the effects of adding successive layers of thin films on a bare silicon chip:

- SMS superstrate where the silicon bulk was 600 μm thick;
- Bare silicon base that was 400 μm thick;
- Silicon base (400 μm thick) with a deposition layer of silicon nitride (400 nm thick);
- Silicon base (400 μm thick) with two deposited layers of silicon nitride (400 nm thick) and aluminum (400 nm thick);

The results of particle patterning on the SMS superstrate are presented in Fig. 4 and Video S1, while the results with respect to the latter three superstrates are organized in S5 of the supplementary material. Three different IDT pitches (100 μm, 200 μm, 300 μm) were employed separately for patterning experiments. The same RF power of 35 dBm was applied. Overall, we can see from Fig. 4 that the average separation distance between patterned particles on the SMS superstrate scales in proportional to the IDT pitch. A pitch of 100 μm (corresponding to a frequency of 19.5 MHz) yields a particle separation in the range of 70-100 μm (Fig. 4 (A)). A pitch of 200 μm (corresponding to a frequency of 10.13 MHz) yields a particle separation in the range of 140-200 μm (Fig. 4 (B)). As such, there is a notable difference between the separation distance and the IDT pitch. In a single-device setup (i.e., direct manipulation of particles on the SAW device), the particle separation distance is typically equal to the IDT pitch. As shown in Fig. 4(C), particles could also be patterned in 2D by generating acoustic waves from two sides at 90° to each other (Fig. 3(C)). PS and silica beads with diameters of 9 μm were separately patterned in 2D using a SAW device with an IDT pitch of 300 μm; the measured period of the separation distance is about 350-400 μm both for PS and silica beads. This separation distance is about √2 times of the separation distance associated with generating waves from all four sides (294-420 μm). This √2 factor of difference matches the simulation results in Fig. 3(B) and 3(C).

B. Lamb wave to Rayleigh wave conversion on multilayer-thin -filmed superstrate

As elaborated in S6 of the supplementary material, the Rayleigh-Lamb characteristic frequency equations were adapted to determine the phase velocity of Lamb waves in silicon. Within the working frequency range of the standard IDTs employed (10.13 MHz and 19.5 MHz), the phase velocity of the two fundamental modes (symmetric (S0) and asymmetric

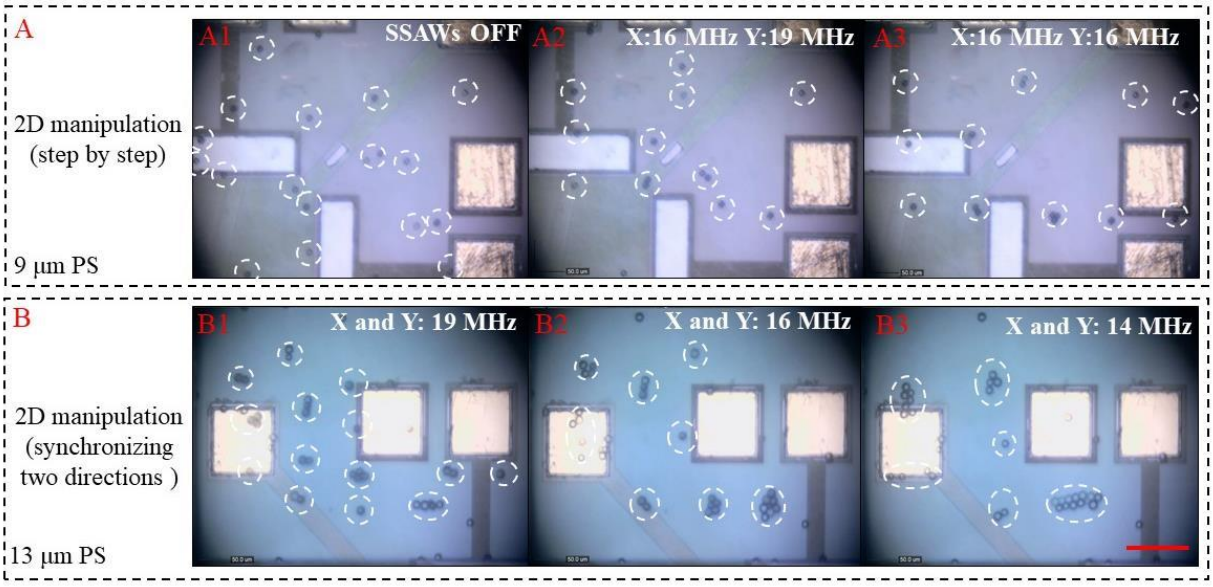

Fig. 6. Controllable manipulation of PS particles in different diameters using chirped IDTs. (A) 2D manipulation of 9 μm PS particles by tuning the frequencies in X and Y independently. The particles firstly arbitrary dispersed (A1), and then trapped and aggregated at the pressure nodes in a 2D array (A2), finally the microbeads were transported to the reconstituted pressure nodes (A3) by only changing the frequency in Y axis. (B) 2D manipulation of larger 13 μm PS microbeads by changing the frequencies in both axes simultaneously starting at 19 MHz (B1), then 16 MHz (B2), and finally 14 MHz (B2). Scale bar: 100 μm.

(A0) modes) are similar in value and fall within the range of 5280-5680 m/s. At an excitation frequency of 19.5 MHz (IDT pitch of 100 μm), this would correspond to a half wavelength of around 135-145 μm on a 600 μm thick silicon slab, which is much larger than the particle separations observed on the SMS superstrate in the patterning experiments (about 70-100 μm). The notable disparity suggests a change in wave type due to the addition of thin-films [23].

To further examine the effect of thin-films on the separation between pressure nodes, particle patterning experiments were performed on a bare silicon superstrate as well as a silicon superstrate with different thin films deposited (all based on 400 μm-thick silicon bases). The phase velocities of the S0 and A0 modes of the Lamb wave on a 400 μm thick silicon slab falls within the range of 5200-5400 m/s at the excitation frequency of 19.5 MHz (corresponding to a half wavelength of around 133-138 μm). As shown in Fig. S4, the measured particle separation for acoustofluidic patterning on bare silicon lies in the range of 110-120 μm (lower than the theoretical half wavelength of a Lamb wave in silicon by 16 %). With a thin silicon nitride layer deposited on the silicon, the measured particle separation reduces to 70-103 μm. Adding a metal layer on the nitride layer does not further change the particle separation distance (found to be 71-106 μm). These separation distances correspond well with the half wavelength of a Raleigh wave based on a computed wave velocity of 4400 m/s for a similar setup and working frequency range [23], though lower by an average of 25%. It is worth noting that the particle separation distance on the SMS superstrate falls in the same range as the silicon superstrate with nitride and nitride/metal films. As such, these results indicate that in the limit where the surface films are much thinner than the bulk material, the properties and details of these surface films make little difference on the particle separation distance. Therefore, these results could be extended to a broad range of microfabricated silicon chips comprising multilayers of patterned films. The slight theoretical overestimate is reasonable if one factors for water loading effects (which are complex to model accurately) known to lower the wave velocity [32].

The Raleigh wave phase velocity for a monolithic layer is constant but dispersive for layered structures, such as thin films deposited on bulk silicon [33]. The Rayleigh velocity dispersion is greatly dependent on the combined effects of wave velocities and densities associated with the substrate and constituent layers. In the case of the SMS superstrate (as well as the bulk silicon with nitride and nitride/metal films), the added thin films are much thinner than the bulk and thus have little effect on the Rayleigh velocity on the silicon superstrate [34]. This outcome is specific to the examples in this paper and should not be generalized, especially in cases of thicker films. In brief, the reason for Rayleigh waves existing on a silicon superstrate deposited with one/two thin films or multilayer thin films (e.g., SMS superstrate) is due to acoustic wave reflection through the bulk. These reflections at the bulk-silicon/nitride interface result from the mismatch in specific acoustic impedances at the interface [23]:

$$Z_{a,i} = \rho_i c_i \quad (3)$$

where i is the phase, ρ_i is the density of layer material, c_i is the velocity of sound, two calculated impendences are: $z_a \approx 36 \times 10^6$ Pa·s·m^{-1} (silicon nitride) and $z_a \approx 19.6 \times 106$ Pa·s·m^{-1} (silicon) [35].

C. Particles moving velocity analysis

The ARF depends on the acoustic pressure, particle volume, distance from pressure nodes and frequency. And increasing the diameter of particles enlarges the ARF. This force-scaling is important in the context of biological applications. For example, the diameter of a tumor cell is about 10-20 μm [29], a scale that works well for acoustic tweezers. First, we compared the velocity of particles under three setups:

• Direct manipulation on the SAW device (i.e., microchamber was bonded on the LN substrate);

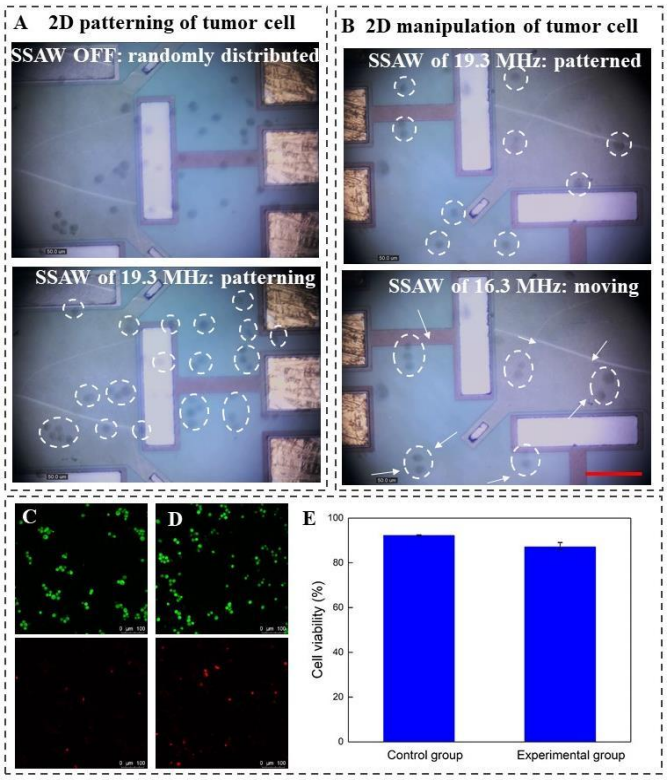

Fig. 7. Demonstration of tumor cells and viability test. (A) Patterning of the human breast cancerous cells with the periods of about 60-80 μm using the chirped IDTs. (B) 2D manipulation of the tumor cells. (C-D) the fluorescence images of collected tumor cells for the control groups (without acoustic treatment) and experimental group (with acoustic treatment of 35 dBm). (C): almost all of the cells emit green fluorescence, while a few sample emit red fluorescence; (D): there was only slight higher intensity of the red fluorescence in experimental group. (E) Quantitative analysis of cell viability for each group. N ≥3. Scale bar: 100 μm.

- Two-chip manipulation on a bare silicon superstrate;
- Two-chip manipulation on the SMS superstrate;

Fig. 5(A-B) records the average velocity of 9 μm PS microbeads as the input RF power was increased 31 dBm to 39 dBm during a 1D patterning process. At a frequency of 10.13 MHz (IDT pitch of 200 μm) with an input power of 39 dBm, the average velocity reaches about 425 μm/s (direct manipulation on the SAW device), 42 μm/s (two-chip manipulation on a bare silicon superstrate) and 24.24 μm/s (two-chip manipulation on the SMS superstrate). These results indicate a drop of more than 90% in the particle travel velocity moving from direct manipulation to two-chip manipulation. Nonetheless, the generated ARF is still enough for biological applications of cell handling.

Next, we compared the velocity of particles in relation to their diameter. Fig. 5 (C) compares the average velocities of different PS microbead diameters measured as the input RF power was increased from 29 dBm to 37 dBm during a 2D patterning process. Keeping the input power fixed at 37 dBm and the frequency at 10.13 MHz, the average velocity reached about 50 μm/s for 13 μm diameter PS beads, 25 μm/s for 9 μm diameter PS beads, and 18 μm/s for 5 μm diameter PS beads. In addition, to compare the effect of particle density on the particle travel velocity, we also measured the average velocity of 9 μm diameter silica microbeads. These results agree with theory, in that a larger particle size correlates with higher travel velocity. In comparison to the size effect, the effect of particle density on velocity is much less notable, although lighter particles generally move faster. Fig. 5(D) summarizes the effect of different excitation frequencies on the ARF based on a comparison of average particle velocities. The average velocity and patterning times were measured during a 1D or 2D manipulation process with an RF power of 35 dBm. Higher excitation frequency is correlated with higher travel velocity and shorter patterning time (time taken for particles to move from their original position and settle into the new pressure nodes), suggesting an increase in the underlying ARF.

D. 2D manipulation of microbeads

Applying standing acoustic waves at a given frequency, the particles were first trapped and aggregated at the nearest pressure nodes on the SMS superstrate. The frequency of the acoustic wave was then modified, thus shifting the positions of the pressure nodes, thereby transporting the aggregated particles to the new pressure nodes. As observed in the video S2, particles within the same cluster do not all move together to the new pressure node with the change of wave frequency. Instead, some of the particles disperse from the cluster and aggregate at new clusters. As shown in Fig. 6(A), in the absence of acoustic waves (ends of the feeding tubes to the microchannel sealed), 9 μm PS microbeads were randomly dispersed in the closed microchamber (Fig. 6(A1)). In applying acoustic waves with an input RF power of 35 dBm (Fig. 6(A2)), the microbeads were first trapped and then cluster at the pressure nodes in a 2D array. In the case of Fig. 6(A2), the excitation frequencies in the X and Y axes were slightly different to illustrate the effect of tuning the frequencies in X and Y independently: X axis (16 MHz), Y axis (19 MHz). Next, the frequency in Y was tuned down to 16 MHz (Fig. 6(A3)). As an additional experiment, Fig. 6(B) shows the manipulation of larger 13 μm PS microbeads as the frequencies in both axes were changed simultaneously starting at 19 MHz (Fig. 6(B1)), then 16 MHz (Fig. 6(B2)), and finally 14 MHz (Fig. 6(B3)). The microbeads did not all follow the same direction of movement upon tuning the frequency. Offsetting the center of the microchamber from the center of the SAW delay line would enable the particles to move in the same direction [26, 29].

We have verified that the particles remain in position after switching off the actuation field (with the inlet and outlet tubes remaining clamped) and transferring the two-chip device to another location. Therefore, the chip can be separately probed after particle manipulation. Alternatively, adding connecting wires to the periphery of the chip outside the microchamber would not visibly alter the particle separation period within the microfluidic chamber.

E. Tumor cells demonstration and viability test

To test the biocompatibility of our device, heating effects were examined by measuring the temperature on the SAW device and on the SMS superstrate. As shown in Fig. S6, when an RF power of 35 dBm was applied to the SAW device, the temperature on the SMS superstrate increased by < 1°C in 30 s. In a longer cell manipulation period, we discretize the exposure times into smaller periods of 30 s to limit the heat increase during each activation period as well as introduce time breaks

of 30 s for cooling between consecutive activation periods [36].

To demonstrate the bio-feasibility of the acoustofluidic platform, we applied our platform to pattern and manipulate tumor cells. As shown in Fig. 7(A-B), the human breast cancerous cells were randomly dispersed in the microchamber initially in the absence of an acoustic field. Once the 2D acoustic field was applied (19.3 MHz, 35 dBm RF power in both axes), the tumor cells were trapped and gathered at the pressure nodes. Moving the visual field of the microscope to inspect other areas of the microchamber, we could visualize the movement of tumor cells to newly formed pressure nodes when the frequency was tuned from 19.3 MHz to 16.3 MHz.

To investigate the impact of high-power acoustic treatment on the integrity of live cells, a short-term cell viability was examined after flowing the cells (at a rate of 100 μL/min) through the microfluidic chamber with an acoustic field applied (RF power of 35 dBm, 19.3 MHz; same parameters as the 2D manipulation experiments on cells above). After all the tumor cell samples had been flowed through the microchannel, the cells collected from the outlets were then stained with imaging solution for 20 min to determine their viability, counting the live cells with emitting green fluorescence and the dead cells with emitting red fluorescence. The fluorescence micrograph of the viability of the tumor cells collected at the outlet is shown in Fig. 7(C-D). Fig. 7(E) compares the cell viability from the control group (92.1%) and from the acoustic treatment (87.1%). As such, a high proportion of the tumor exposed to acoustic treatment remained alive during the short-term viability test. The results indicate that exposure of the tumor cells to acoustic treatment for cell manipulated caused little harm to the cells compared to tumor cells cultured in an incubator.

V. Conclusions

In this work, we have demonstrated acoustically driven 2D patterning and manipulation of particles and cells on a surface micromachined silicon (SMS) chip, advancing the application of acoustofluidic methods from simple bare superstrates or direct manipulation on a SAW device. The periodic separating distance between particles on the SMS superstrate indicate that the pressure field on the chip is possibly defined by Raleigh waves instead of Lamb waves. These findings are applicable to a broad range of microfabricated devices. The dependence on multiple parameters including RF driving power and frequency, particle and density were documented. To further demonstrate the biocompatibility of manipulation on the SMS superstrate, we have applied the method to manipulate human breast cancer cells and demonstrated high cell viability (87.1%). This research lays the groundwork of extending acoustically driven manipulation methods to functional chips toward a label-free, contactless, highly-dexterous, comparatively low-cost and biocompatible tool for biomedical sample handling.

References

[1] J. Shi, H. Huang, Z. Stratton, Y. Huang, and T. J. Huang, "Continuous particle separation in a microfluidic channel via standing surface acoustic waves (SSAW)," *Lab Chip*, vol. 9, pp. 3354-3359, 2009.

[2] Y. Bourquin, A. Syed, J. Reboud, L. C. R. Cartwright, M. P. Barrett, and J. M. Cooper, "Rare-cell enrichment by a rap-id, label-free, ultrasonic isopycnic technique for medical diagnostics," *Angew. Chem. Int. Ed.*, vol. 53, pp. 5587-5590, 2014.

[3] P. Li, Z. Mao, Z. Peng, L. Zhou, Y. Chen, P. Huang, C. I. Truica, J. J. Drabick, W. S. El-Deiry, M. Dao, S. Suresh, and T. J. Huang, "Acoustic separation of circulating tumor cells," *PNAS*, vol. 112, pp. 4970-4975, 2015.

[4] J. Shi, D. Ahmed, X. Mao, S. S. Lin, A. Lawit, T. J. Huang, "Acoustic tweezers: patterning cells and micro-particles using standing surface acoustic waves (SSAW)," *Lab Chip*, vol. 9, pp. 2890-2895, 2009.

[5] H. Bruus, J. Dual, J. Hawkes, M. Hill, T. Laurell, J. Nilsson, S. Radel, S. Sadhal, and M. Wiklund, "Forthcoming lab on a chip tutorial series on acoustofluidics: acoustofluidics-exploiting ultrasonic standing wave forces and acoustic streaming in microfluidic systems for cell and particle manipulation," *Lab Chip*, vol. 11, pp. 3579-3580, 2011.

[6] X. Ding, P. Li, S. C. S. Lin, Z. S. Stratton, N. Nama, F. Guo, D. Slotcavage, X. Mao, J. Shi, F. Costanzo, and T. J. Huang, "Surface acoustic wave microfluidics," *Lab Chip*, vol. 13, pp. 3626-3649, 2013.

[7] A. Ozcelik, J. Rufo, F. Guo, Y. Gu, P. Li, J. Lata, and T. J. Huang, "Acoustic tweezers for the life sciences," *Nat. Methods*, vol. 15, pp. 1021-1028, 2018.

[8] M. Wu, P. H. Huang, R. Zhang, Z. Mao, C. Chen, G. Kemeny, P. Li, A. V. Lee, R. Gyanchandani, A. J. Arm-strong, M. Dao, S. Suresh, and T. J. Huang, "Circulating tumor cell phenotyping via high-throughput acoustic separation," *Small*, vol. 14, pp. 1801131, 2018.

[9] S. P. Zhang, J. Lata, C. Chen, J. Mai, F. Guo, Z. Tian, L. Ren, Z, Mao, P. H. Huang, P. Li, S. Yang, and T. J. Huang, "Digital acoustofluidics enables contactless and programmable liquid handling," *Nat. Commun*., vol. 9, pp. 2928, 2018.

[10] D. J. Collins, B. Morahan, J. G.-Bustos, C. Doerig, M. Plebanski, and A. Neild, "Two-dimensional single-cell patterning with one cell per well driven by surface acoustic waves," *Nat. Commun.*, vol. 6, pp. 8686, 2015.

[11] W. Connacher, N. Zhang, A. Huang, J. Mei, S. Zhang, T. Gopesh, and J. Friend, "Micro/nano acoustofluidics: materials, phenomena, design, devices, and applications," *Lab Chip*, vol. 18, pp. 1952-1996, 2018.

[12] P. Zhang, H. Bachman, A. Ozcelik, and T. J. Huang, "Acoustic microfluidics," *Annual Review of Analytical Chemistry*, vol. 13, pp. 17-43, 2020.

[13] C. Witte, J. Reboud, R. Wilson, J. M. Cooper, and S. L. Neale, "Microfluidic resonant cavities enable acoustophoresis on a disposable superstrate," *Lab Chip*, vol. 14, pp. 4277-4283, 2014.

[14] S. Zhao, M. Wu, S. Yang, Y. Wu, Y. Gu, C. Chen, J. Ye, Z. Xie, Z. Tian, H. Bachman, P. H. Huang, J. Xia, S. P. Zhang, H. Zhang, and T. J. Huang, "A disposable acoustofluidic chip for nano/micro particle separation using unidirectional acoustic transducers," *Lab Chip*, vol. 20, pp. 1298-1308, 2020.

[15] Z. Tian, S. Yang, P.-H. Huang, Z. Wang, P. Zhang, Y. Gu, H. Bachman, C. Chen, M. Wu, Y. Xie, and T. J. Huang, "Wavenumber-spiral acoustic tweezers for dynamic and reconfigurable manipulation of particles and cells," *Science Advances*, vol. 5, pp. eaau6062, 2019.

[16] F. Guo, Y. Xie, S. Li, J. Lata, L. Ren, Z. Mao, B. Ren, M. Wu, A. Ozcelik, and T. J. Huang, "Reusable acoustic tweezers for disposable devices," *Lab Chip*, vol. 15, pp. 4517-4523, 2015.

[17] Y. Bourquin, J. Reboud, R. Wilson, Y. Zhang, and J. M. Cooper, "Integrated immunoassay using tuneable surface acoustic waves and lensfree detection," *Lab Chip*, vol. 11, pp. 2725-2730, 2011.

[18] D. Mampallil, J. Reboud, R. Wilson, D. Wylie, D. R. Klug, and J. M. Cooper, "Acoustic suppression of the coffee-ring effect," *Soft matter*, vol. 11, pp. 7207-7213, 2015.

[19] G. Destgeer, and H. J. Sung, "Recent advances in micro-fluidic actuation and micro-object manipulation via sur-face acoustic waves," *Lab Chip*, vol. 15, pp. 2722-2738, 2015.

[20] Y. Bourquin, J. Reboud, R. Wilson, and J. M. Cooper, "Tuneable surface acoustic waves for fluid and particle manipulations on disposable chips," *Lab Chip,* vol. 10, pp. 1898-1901, 2010.

[21] J. Reboud, Y. Bourquin, R. Wilson, G. S. Pall, M. Jiwaji, A. R. Pitt, and J. M. Cooper, "Shaping acoustic fields as a toolset for microfluidic manipulations in diagnostic technologies," *PNAS*, vol. 109, pp. 15162-15167, 2012.

[22] R. Wilson, J. Reboud, Y. Bourquin, S. L. Neale, Y. Zhang, and J. M. Cooper, "Phononic crystal structures for acoustically driven microfluidic manipulations," *Lab Chip*, vol. 11, pp. 323-328, 2011.

[23] K. S. Wong, L. Lee, Y. M. Hung, L. Y. Yeo, and M. K. Tan, "Lamb to Rayleigh wave conversion on superstrates as a means to facilitate disposable acoustomicrofluidic applications," *Anal. Chem.*, Vol. 91, pp. 12358-12368, 2019.

[24] Z. Ma, D. J. Collins, Y. Ai, "Detachable acoustofluidic system for particles separation via a traveling surface acoustic wave," *Anal. Chem.*, Vol. 88, pp. 5316-5323, 2016.
[25] P. Li, Z. Ma, Y. Zhou, D. J. Collins, Z. Wang, Y. Ai, "Detachable acoustophoretic system for fluorescence-activated sorting at the single droplet level," *Anal. Chem.*, Vol. 91, pp. 9970-9977, 2019.
[26] J. Qian, J. Ren, Y. Liu, R. H. W. Lam, and J. E.-Y. Lee, "Two-chip acoustofluidic particle manipulation platform with a detachable and reusable surface acoustic wave device," *Analyst*, vol. 145, pp. 7752-7758, 2020.
[27] R. P. Hodgson, M. Tan, L. Yeo, and J. Friend, "Trans-mitting high power rf acoustic radiation via fluid couplants into superstrates for microfluidics," *Appl. Phys. Lett.*, vol. 94, pp. 024102, 2009.
[28] X. Ding, J. Shi, S.-C. S. Lin, S. Yazdi, B. Kiraly, and T. J. Huang, "Tunable patterning of microparticles and cells using standing surface acoustic waves," *Lab Chip*, vol. 12, pp. 2491-2497, 2012.
[29] X. Ding, S.-C.S. Lin, B. Kiraly, H. Yue, S. Li, I-K. Chiang, J. Shi, S. J. Benkovic, and T. J. Huang, "On-chip manipulation of single microparticles, cells, and organisms using surface acoustic waves," *PNAS*, vol. 109, pp. 11105-11109, 2012.
[30] F. Guo, Z. Mao, Y. Chen, Z. Xie, J. P. Lata, P. Li, L. Ren, J. Liu, J. Yang, M. Dao, S. Suresh, and T. J. Huang, "Three-dimensional manipulation of single cells using surface acoustic waves," *PNAS*, vol. 113, pp. 1522-1527, 2016.
[31] Y. Xie, Z. Mao, H. Bachman, P. Li, P. Zhang, L. Ren, M. Wu, and T. J. Huang, "Acoustic cell separation based on density and mechanical properties," *Journal of Biomechanical Engineering*, vol. 142, pp. 031005, 2020.
[32] R. M. White, and S. W. Wenzel, "Fluid loading of a Lamb-wave sensor," *Appl. Phys. Lett.,* vol. 52, pp. 1653, 1988.
[33] A. A. Tarasenkoa, L. Jastrab`ık, and N. A. Tarasenko, "Effect of roughness on the elastic surface wave propagation," *Eur. Phys. J. Appl. Phys.*, vol. 24, pp. 3-12, 2003.
[34] I. Beldi, Hadjoub, A. Doghmane, and A. Gacem, "Investigation of anomalous behavior of positive SAW velocity dispersion curves for water/layers/silicon systems," *WCU 2003*, Paris, September 7-10, 2003. Available: http://www.univ-tebessa.dz/fichiers/skikda/000166.pdf
[35] Signal Processing, Technique tables. [Online]. Available: https://www.signal-processing.com/table.php.
[36] A. Ozcelik, N. Nama, P.-H. Huang, M. Kaynak, M. R. McReynolds, W. Hanna-Rose, and T. J. Huang, "Acoustofluidic rotational manipulation using oscillating solid structures," *Small*, vol. 12, pp. 5120-5125, 2016.

Jingui Qian received the BS degree from Wenzhou University, China in 2015 and MS degree from Chonnam National University, Republic of Korea in 2017. Thereafter, he joined the Hong Kong Polytechnic University as Research Assistant. He is currently working toward the PhD degree in the Department of Electrical Engineering, City University of Hong Kong. His research interest includes acoustofluidics, nanogenerators, sensors and resonators, self-powered system.

Jifeng Ren received the B.Eng. degree from Chongqing Jiaotong University, China in 2015 and M.Sc degree from University of Birmingham, U.K. in 2016. He is currently presuming his PhD degree in City University of Hong Kong. His research interest includes microfluidic chips, cell mechanics, and finite element analysis of laser ablation and laminar flow.

Wei Huang received his BS degree from Northwest A&F University, China in 2016 and MSc degree from City University of Hong Kong, Hong Kong in 2018. He is currently working toward the PhD degree in the Department of Biomedical Engineering at City University of Hong Kong. His research interest includes microfluidics, cell Mechanics, cancer stem cells, and biosensors.

Dr. Raymond H. W. Lam received the B. Eng. and M. Phil degrees from Chinese University of Hong Kong, and received the PhD degree from the Massachusetts Institute of Technology. He is currently an Associate Professor of Biomedical Engineering at City University of Hong Kong. His research focuses on microfluidics, cell biomechanics, microbioreactors, and microengineering.

Dr. Joshua E.-Y. Lee received the B.A. (Hons) and M. Eng. (Distinction) degrees in 2005, and the Ph.D. degree in 2009, from the University of Cambridge, U.K. Since June 2009, he has been a faculty of the Department of Electrical Engineering, City University of Hong Kong at the level of Associate Professor and affiliated with the State Key Laboratory of Millimeter Waves. He is currently Principal Scientist at the Institute of Microelectronics, A*STAR, Singapore. In 2017, he was a visiting professor at University Grenoble Alpes in France. His research interests include the design, analysis, and characterization of Microelectromechanical Systems (MEMS) for sensing and frequency control applications. Dr Lee is a Senior Member of the IEEE. He has served on the Technical Program Committees of various conferences including ISQED, IFCS, and Transducers.